Predictive Control of Bidirectional Voltage Source Converter With Reduced Current Harmonics and Flexible Power Regulation Under Unbalanced Grid

Nan Jin, *Member, IEEE*, Chun Gan, *Member, IEEE*, and Leilei Guo

***Abstract*—This paper proposes a simplified and improved model predictive current control (MPCC) scheme for grid-connected bidirectional voltage source converter (GC-BVSC) when the unbalanced grid voltages occur. In conditions of unbalanced grid voltage, the current harmonic components of the GC-BVSC increase significantly, and twice grid-frequency ripple exist in both active power and reactive power, which influence the output power quality. To reduce harmonic currents and power fluctuations, an improved MPCC (IMPCC) method is proposed, and a two-step predictive model of GC-BVSC is put forward. The current compensation values are expressed by grid voltages and their quadrature signals that lag 90 electrical degrees in the $\alpha\beta$ stationary coordinates system. The cost function reducing both the power ripple and current distortion is designed. Compared to conventional methods, phase-locked loop, pulse width modulation, and complex positive and negative sequence extraction of grid voltage are not required. In addition, IMPCC presents a better performance by reducing both grid-connected current harmonics and power ripple of GC-BVSC with flexible bidirectional power regulation capability. Simulation and experimental results on power electronics-professional (PE-PRO) platform verify the effectiveness of the proposed scheme under both single-phase and three-phase unbalanced grid voltages.**

***Index Terms*—Grid-connected bidirectional voltage source converter (GC-BVSC), unbalanced grid voltages, predictive control, current harmonics, power regulation.**

I. Introduction

DUE to the increasing use of DC distributed power sources, such as photovoltaic (PV) panels, fuel cells, and batteries, bidirectional power conversion has become an urgent issue for power management and control systems. Microgrids are an effective means to connect the power grid and distributed power generation [1]–[3], which have been widely concerned to improve the efficiency of the clean energy power generation. As the key equipment to control power conversion in hybrid microgrids, the reliable and stable operation of grid-connected bidirectional voltage source converter (GC-BVSC) is vital to the power flow stability in microgrids [3]–[8]. The harmonic contents of grid currents and power ripple are significantly increased under unbalanced grid voltage, which will influence the power quality [9], [10]. Therefore, it is necessary to investigate the control methods of GC-BVSC under grid voltage conditions.

In early research, the conventional control methods of GC-BVSC generate control signals using pulse width modulation (PWM) and voltage oriented control (VOC). In VOC, the grid current is extracted by active power components i_d and reactive power components i_q. Then the d–q components of grid currents are controlled separately by proportional integral (PI) control technique. The external voltage loop controls DC voltage and the inner current loop controls grid current. The unbalanced grid voltages have been considered to be one of the challenges for the control of the GC-BVSC to achieve good performance, when the power converter is connected to the AC grid. Under unbalanced grid conditions, investigations have been conducted to eliminate the power ripples and reduce the current harmonics. Sequence extraction of the grid voltage and current is used to decompose the positive/negative components [11]. However, the calculation burden is large, and the negative-current is difficult to control. The control techniques which can regulate the positive and negative current have been investigated in [12], [13], while the control performances are not satisfactory. The gird currents are highly distorted and the power oscillations still exist. Grid synchronization has also become a problem in the condition of unbalanced grid voltages, and dual second-order generalized integrator (SOGI) phase locked loop is developed to estimate the instantaneous symmetrical components of the grid voltage [14]. The twice line-frequency power ripples in both active power and reactive power significantly affect the power quality. In particular, it has been proven that the power ripples can be eliminated by accepting highly distorted currents [15]. Therefore, under unbalance grid conditions, phase locked loop (PLL) is necessary for VOC to separate the positive and negative sequence of voltage and current. Multi PI controllers and pulse width modulation (PWM) to regulate the sequence current components. The calculation amount is large, and the control strategy is complex.

Manuscript received May 15, 2017; revised August 29, 2017 and November 14, 2017; accepted November 29, 2017. Date of publication December 11, 2017; date of current version August 17, 2018. This work was supported in part by the National Natural Science Foundation of China under Grants 51607159 and U1604136, in part by the Science and Technology Innovation Talents in Universities of Henan Province (18HASTIT025 and 2015GGJS-180), and in part by the Scientific and Technological Project in Henan Province (172102410068). Paper no. TEC-00380-2017. *(Corresponding author: Chun Gan.)*

N. Jin and L. Guo are with the College of Electric and Information Engineering, Zhengzhou University of Light Industry, Zhengzhou 450002, China (e-mail: jinnan@zzuli.edu.cn; 2006guoleilei@163.com).

C. Gan is with the Department of Electrical Engineering and Computer Science, University of Tennessee, Knoxville, TN 37996 USA (e-mail: cgan@utk.edu).

Color versions of one or more of the figures in this paper are available online at http://ieeexplore.ieee.org.

Digital Object Identifier 10.1109/TEC.2017.2781692

Direct power control (DPC) is a kind of high-performance control strategy for the PWM converter [16], which is similar to the direct torque control in motor drives. Compared to the VOC, the DPC directly selects the desired voltage vector from a predefined switching table and eliminates the internal current loop. As a result, the dynamic response is fast. However, the switching table in the conventional DPC is obtained in a heuristic way, which cannot ensure the effectiveness of the selected voltage vector. Therefore, the conventional switching table is improved to achieve the performance improvement by developing new switching tables [17]. A method to express the active power and reactive power by grid voltages and currents with their quadrature signals is proposed in [18]. In [19] and [20], power compensations are added to the reference active or reactive power to improve the performance, but they still require complex positive and negative sequence separation. A new type of DPC with model predictive method (MPDPC) is proposed under unbalanced grid voltages [21]. This approach achieves low switching frequency, whereas it obtains lower power ripple. According to [21], the new defined reactive power, used as a control variable, is more suitable than the conventional reactive power. Constant active power can be achieved under both balanced and unbalanced grid voltage conditions without grid current distortion. A model predictive direct power control with low-complexity and power compensation strategy for doubly fed induction generator (DFIG) under both balanced and unbalanced grid conditions was proposed in [22]. However, the phase-locked loop (PLL) and sequence extraction are required.

Model predictive current control (MPCC) has the advantages of its flexible capability to control different types of variables and include constraints in a simple way [23]. According to the mathematical model of three-phase grid-connected inverters, a model-predictive current control method [24] is proposed in the two-phase static $\alpha\beta$-frame. Based on the principle of model predictive control, a predictive current model is established by using coordinates transformation to assess different voltage vectors of inverters and predict all possible output values. The voltage vector which minimizes the cost function is selected. Then the corresponding switching state is applied at the next sampling time to track the reference current. In addition, to solve the problem of the delay between the measurements and the actuation, delay compensation method is proposed to improve the performance [25]. However, the existing MPCC method is mainly applied under balanced grid voltages. In the conditions of unbalanced voltages, the harmonic currents and power ripples will increase significantly. The model predictive current control (MPCC) also needs further study.

Model predictive control advantages include an accurate and effective selection of voltage vectors [26]–[29], [31]–[35]. In this paper, an improved and simplified model predictive current control (IMPCC) method is proposed to GC-BVSC under unbalanced power grid with low current harmonics distortion and flexible power regulation capability. The main contributions of this paper are as follows. First, reference currents are expressed with grid voltages and their quadrature signals, which are different from the conventional expression using the positive and negative sequence components. Second, the cost function includes both power ripple terms and current distortion terms. By selecting the best voltage vector to minimize the cost function, the IMPCC method shows better steady-state and dynamic performance. Without the Park transformation, extraction of current positive and negative sequence components and PLL, the harmonic contents of grid current are reduced and active power or reactive power ripple are eliminated by using the proposed IMPCC. Third, the proposed method can regulate the active power and reactive power at the same time under unbalanced grid voltages conditions. According to [30], the current limited control strategy for the proposed IMPCC is designed for the safe operation, and flexible reactive power generation is achieved in fault ride-through (FRT) condition. Comparisons are made between the proposed and conventional methods. The transition between different working modes is investigated to analyze the dynamic performance in bidirectional power conversion. Simulation and experiments are carried out to verify the effectiveness of the proposed control strategy.

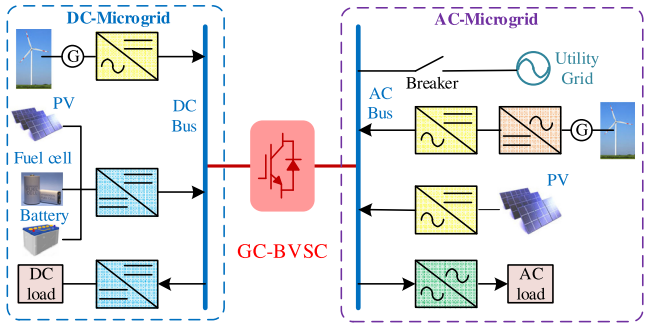

Fig. 1. Structure of hybrid microgrids with GC-BVSC.

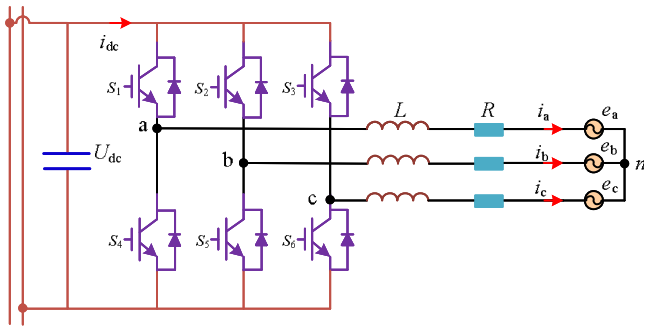

Fig. 2. Equivalent circuit of GC-BVSC.

II. Predictive Model of GC-BVSC

As the connection between DC grid and AC grid, GC-BVSC can achieve bidirectional power flow between them. The structure of hybrid microgrids is shown in Fig. 1.

According to the active power flow direction, GC-BVSC has two modes of grid-connected operation: inverter mode and rectifier mode. In the inverter mode, the active power flows from the DC side to AC side, and vice versa in rectifier mode. The equivalent circuit of GC-BVSC is shown in Fig. 2. U_{dc}, L, R are the DC voltage, filter inductance, and equivalent series

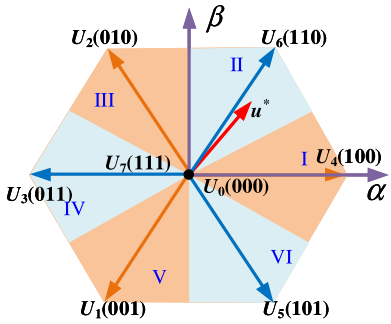

Fig. 3. Sector distribution of space voltage vector.

resistance, respectively. e_a, e_b, e_c, i_a, i_b, i_c are the grid-connected voltages and currents.

According to the Kirchhoff law, the state equation of GC-BVSC in abc three-phase static coordinates system can be expressed as:

$$L\frac{\mathrm{d}}{\mathrm{d}t}\begin{bmatrix} i_a \\ i_b \\ i_c \end{bmatrix} + R\begin{bmatrix} i_a \\ i_b \\ i_c \end{bmatrix} = \begin{bmatrix} u_{an} \\ u_{bn} \\ u_{cn} \end{bmatrix} - \begin{bmatrix} e_a \\ e_b \\ e_c \end{bmatrix} \tag{1}$$

where u_{an}, u_{bn}, u_{cn} are the three-phase output voltage.

Using Clark transformation, the state equation in $\alpha\beta$ two phase stationary coordinates is obtained by (1).

$$L\frac{\mathrm{d}}{\mathrm{d}t}\begin{bmatrix} i_\alpha \\ i_\beta \end{bmatrix} + R\begin{bmatrix} i_\alpha \\ i_\beta \end{bmatrix} = \begin{bmatrix} u_\alpha \\ u_\beta \end{bmatrix} - \begin{bmatrix} e_\alpha \\ e_\beta \end{bmatrix} \tag{2}$$

where i_α, i_β, u_α, u_β, e_α, e_β are α, β components of converter output currents, voltages and grid voltages, respectively.

The switching state of the BVSC S_i $(i = \mathrm{a}, \mathrm{b}, \mathrm{c})$ is defined as follows

$$S_i = \begin{cases} 1 & \text{Upper bridge of phase } i \text{ is on and lower bridge is off} \\ 0 & \text{Upper bridge of phase } i \text{ is off and lower bridge is on} \end{cases} \tag{3}$$

There are eight switching states in the converter: (0 0 0), (0 0 1), (0 1 0), (1 1 0), (1 0 0) (1 0 1), (1 1 0), (1 1 1). The converter output voltage vectors $\boldsymbol{U}_j$ $(j = 0 - 7)$ are shown in Fig. 3, where $\boldsymbol{U}_0$ and $\boldsymbol{U}_7$ are zero vector.

The relationship between output voltage and switching state is shown as

$$\begin{bmatrix} u_{an} \\ u_{bn} \\ u_{cn} \end{bmatrix} = \frac{U_{dc}}{3}\begin{bmatrix} 2 & -1 & -1 \\ -1 & 2 & -1 \\ -1 & -1 & 2 \end{bmatrix}\begin{bmatrix} S_a \\ S_b \\ S_c \end{bmatrix} \tag{4}$$

The state equation in $\alpha\beta$ two phase stationary coordinates can be obtained by using Clark transformation of (4).

$$\begin{bmatrix} u_\alpha \\ u_\beta \end{bmatrix} = \frac{\sqrt{6}U_{dc}}{9}\begin{bmatrix} 1 & -\frac{1}{2} & -\frac{1}{2} \\ 0 & \frac{\sqrt{3}}{2} & -\frac{\sqrt{3}}{2} \end{bmatrix}\begin{bmatrix} 2S_a - S_b - S_c \\ -S_a + 2S_b - S_c \\ -S_a - S_b + 2S_c \end{bmatrix} \tag{5}$$

When T_s is the sampling period, (2) can be discretized as

$$\frac{L}{T_s}\begin{bmatrix} i_\alpha(k+1) - i_\alpha(k) \\ i_\beta(k+1) - i_\beta(k) \end{bmatrix} = \begin{bmatrix} u_\alpha(k) \\ u_\beta(k) \end{bmatrix} - R\begin{bmatrix} i_\alpha(k) \\ i_\beta(k) \end{bmatrix} - \begin{bmatrix} e_\alpha \\ e_\beta \end{bmatrix} \tag{6}$$

Predictive currents are expressed as

$$\begin{bmatrix} i_\alpha(k+1) \\ i_\beta(k+1) \end{bmatrix} = \frac{T_s}{L}\begin{bmatrix} u_\alpha(k) - e_\alpha \\ u_\beta(k) - e_\beta \end{bmatrix} + \left(1 - \frac{RT_s}{L}\right)\begin{bmatrix} i_\alpha(k) \\ i_\beta(k) \end{bmatrix} \tag{7}$$

where $i_\alpha(k)$, $i_\beta(k)$, $u_\alpha(k)$, $u_\beta(k)$, $e_\alpha(k)$, and $e_\beta(k)$ are $\alpha\beta$ components of output currents, voltages and grid voltages at t_k instant. $i_\alpha(k+1)$ and $i_\beta(k+1)$ are $\alpha\beta$ components of predictive current value at t_{k+1} instant.

According to the instantaneous power theory, the complex power S of the grid can be expressed as:

$$S = ei^* = P + jQ \tag{8}$$

where symbol "$*$" denotes the conjugate. The active power and reactive power can be expressed by the following forms:

$$\begin{cases} P = e_\alpha i_\alpha + e_\beta i_\beta \\ Q = e_\beta i_\alpha - e_\alpha i_\beta \end{cases} \tag{9}$$

The predictive model of GC-BVSC at t_{k+1} instant can be obtained by

$$\begin{bmatrix} P(k+1) \\ Q(k+1) \end{bmatrix} = \frac{T_s}{L}\begin{bmatrix} e_\alpha & e_\beta \\ e_\beta & -e_\alpha \end{bmatrix}\begin{bmatrix} u_\alpha(k) - e_\alpha - Ri_\alpha(k) \\ u_\beta(k) - e_\beta - Ri_\beta(k) \end{bmatrix} + \begin{bmatrix} P(k) \\ Q(k) \end{bmatrix} \tag{10}$$

III. Power Analysis Under Unbalanced Grid Voltage

In the conditions of unbalanced grid voltage conditions, the current harmonic contents of GC-BVSC increase significantly and twice line-frequency ripple exist in both active power and reactive power, which influence the output power quality.

A. Conventional Power Calculation in dq-Axis

In the conditions of unbalanced grid voltages, grid voltages and currents can be expressed as the sum of positive and negative sequence components:

$$\begin{cases} e = e_{\alpha\beta}{}^+ + e_{\alpha\beta}{}^- = e_{dq}{}^+ e^{j\omega t} + e_{dq}{}^- e^{-j\omega t} \\ i = i_{\alpha\beta}{}^+ + i_{\alpha\beta}{}^- = i_{dq}{}^+ e^{j\omega t} + i_{dq}{}^- e^{-j\omega t} \end{cases} \tag{11}$$

$$\begin{cases} e_{dq}{}^+ = e_d{}^+ + je_q{}^+ \\ e_{dq}{}^- = e_d{}^- + je_q{}^- \\ i_{dq}{}^+ = i_d{}^+ + ji_q{}^+ \\ i_{dq}{}^- = i_d{}^- + ji_q{}^- \end{cases} \tag{12}$$

where $e^+_{\alpha\beta}$, $e^-_{\alpha\beta}$, e^+_{dq}, e^-_{dq}, $i^+_{\alpha\beta}$, $i^-_{\alpha\beta}$, i^+_{dq}, and i^-_{dq} are the positive and negative sequence components of the grid voltage/current in $\alpha\beta$-*axis* and *dq-axis*, respectively. ω is the angular frequency of grid voltage.

The grid side power can be given by:

$$S = P + jQ = ({e_{dq}}^{+} e^{j\omega t} + {e_{dq}}^{-} e^{-j\omega t}) \times ({i_{dq}}^{+} e^{j\omega t} + {i_{dq}}^{-} e^{-j\omega t})^{*} \tag{13}$$

where

$$\begin{cases} P = p_0 + p_{c2}\cos(2\omega t) + p_{s2}\sin(2\omega t) \\ Q = q_0 + q_{c2}\cos(2\omega t) + q_{s2}\sin(2\omega t) \end{cases} \tag{14}$$

When unbalanced grid voltages occur, (14) shows that there is the twice grid-frequency power ripple existing in the output power. In dq rotating coordinates, by expanding (13) and (14), the expression of output power can be expressed as:

$$\begin{cases} p_0 = {e_d}^{+}{i_d}^{+} + {e_q}^{+}{i_q}^{+} + {e_d}^{-}{i_d}^{-} + {e_q}^{-}{i_q}^{-} \\ p_{c2} = {e_d}^{+}{i_d}^{-} + {e_q}^{+}{i_q}^{-} + {e_d}^{-}{i_d}^{+} + {e_q}^{-}{i_q}^{+} \\ p_{s2} = {e_d}^{+}{i_q}^{-} - {e_q}^{+}{i_d}^{-} + {e_d}^{-}{i_d}^{+} - {e_q}^{-}{i_q}^{+} \\ q_0 = {e_q}^{+}{i_d}^{+} - {e_d}^{+}{i_q}^{+} + {e_q}^{-}{i_d}^{-} - {e_d}^{-}{i_q}^{-} \\ q_{c2} = {e_q}^{+}{i_d}^{-} - {e_d}^{+}{i_q}^{-} + {e_q}^{-}{i_d}^{-} - {e_d}^{-}{i_q}^{+} \\ q_{s2} = {e_d}^{+}{i_d}^{-} + {e_q}^{+}{i_q}^{-} - {e_d}^{-}{i_d}^{+} - {e_q}^{-}{i_q}^{+} \end{cases} \tag{15}$$

where p_0 and q_0 are the average values of active power and reactive power, p_{c2}, p_{s2}, q_{c2} and q_{s2} are the twice grid-frequency ripple in active power and reactive power, respectively.

B. Power Calculation in $\alpha\beta$-Axis

Suppose x is a variable in $\alpha\beta$-*axis*, and its quadrature signals which lag by 90° can be expressed as x'.

$$x' = -jx_{dq}{}^{+}e^{j\omega t} + jx_{dq}{}^{-}e^{-j\omega t} = -jx_{\alpha\beta}{}^{+} + jx_{\alpha\beta}{}^{-} \tag{16}$$

Hence, x and x' can be expressed by positive, negative sequence component $x_{\alpha\beta}{}^{+}, x_{\alpha\beta}{}^{-}$ in $\alpha\beta$-axis, as follows:

$$\begin{bmatrix} x \\ x' \end{bmatrix} = \begin{bmatrix} 1 & 1 \\ -j & j \end{bmatrix} \begin{bmatrix} x_{\alpha\beta}{}^{+} \\ x_{\alpha\beta}{}^{-} \end{bmatrix} \tag{17}$$

The positive and negative sequence components of x in $\alpha\beta$-axis are shown as:

$$\begin{bmatrix} x_{\alpha\beta}{}^{+} \\ x_{\alpha\beta}{}^{-} \end{bmatrix} = \frac{1}{2}\begin{bmatrix} 1 & j \\ 1 & -j \end{bmatrix} \begin{bmatrix} x \\ x' \end{bmatrix} \tag{18}$$

The positive and negative sequence components of x in dq-*axis* can be expressed by x and x', as follows:

$$\begin{bmatrix} x_{dq}{}^{+} \\ x_{dq}{}^{-} \end{bmatrix} = \begin{bmatrix} e^{-j\omega t} & 0 \\ 0 & e^{j\omega t} \end{bmatrix} \begin{bmatrix} x_{\alpha\beta}{}^{+} \\ x_{\alpha\beta}{}^{-} \end{bmatrix} \tag{19}$$

$$\begin{bmatrix} x_{dq}{}^{+} \\ x_{dq}{}^{-} \end{bmatrix} = \frac{1}{2}\begin{bmatrix} e^{-j\omega t} & je^{-j\omega t} \\ e^{j\omega t} & -je^{j\omega t} \end{bmatrix} \begin{bmatrix} x \\ x' \end{bmatrix} \tag{20}$$

According to (15) and (20), active power and reactive power are expressed by grid voltage and current as follows:

$$\begin{cases} p_0 = \frac{1}{2}(i_\alpha e_\alpha + i_\beta e_\beta + i_\alpha{}' e_\alpha{}' + i_\beta{}' e_\beta{}') \\ p_{c2} = \frac{1}{2}\left[k_1\cos(2\omega t) + k_2\sin(2\omega t)\right] \\ p_{s2} = \frac{1}{2}\left[-k_2\cos(2\omega t) + k_1\sin(2\omega t)\right] \\ q_0 = \frac{1}{2}(i_\alpha e_\beta - i_\beta e_\alpha + i_\alpha{}' e_\beta{}' - i_\beta{}' e_\alpha{}') \\ q_{c2} = \frac{1}{2}\left[k_3\cos(2\omega t) + k_4\sin(2\omega t)\right] \\ q_{s2} = \frac{1}{2}\left[-k_4\cos(2\omega t) + k_3\sin(2\omega t)\right] \end{cases} \tag{21}$$

where

$$\begin{cases} k_1 = i_\alpha e_\alpha + i_\beta e_\beta - i_\alpha{}' e_\alpha{}' - i_\beta{}' e_\beta{}' \\ k_2 = i_\alpha e_\alpha{}' + i_\beta e_\beta{}' + i_\alpha{}' e_\alpha + i_\beta{}' e_\beta \\ k_3 = i_\alpha e_\beta - i_\beta e_\alpha - i_\alpha{}' e_\beta{}' + i_\beta{}' e_\alpha{}' \\ k_4 = i_\alpha e_\beta{}' - i_\beta e_\alpha{}' + i_\alpha{}' e_\beta - i_\beta{}' e_\alpha \end{cases} \tag{22}$$

where e_α, e_β, e'_α, e'_β, i_α, i_β, i'_α, and i'_β are the α, β component of grid voltage, current and their quadrature signals, respectively.

IV. IMPCC Method Under Unbalanced Grid Voltage Faults

In the conditions of unbalanced grid voltage fault, phase locked loop (PLL) technology is used to separate the positive and negative sequence of voltage and current [23]. A method is proposed to express active power and reactive power by using grid voltages and currents with their quadrature signals. Therefore, without extraction of sequence components, the simplified method is easier to realize [24]. However, only constant active power from the DC to AC side is mainly achieved. In this paper, an improved IMPCC method for GC-BVSC to achieve bidirectional power conversion between AC and DC sides is proposed, and the flexible bidirectional power regulation and elimination of power ripple are also investigated. The current reference value i_{ref} can be calculated by solving (21) with different control objectives.

A. Reference Current Calculation of Flexible Power Regulation With Active Power Ripple Elimination

If the control objective is to eliminate active power ripple, p_{c2} and p_{s2} in the corresponding formula (21) are 0. The coefficients k_1 and k_2 are 0. In order to regulate the active and reactive power simultaneously, the following equation should be solved.

$$\begin{cases} p_0 = P_{ref} \\ q_0 = Q_{ref} \\ k_1 = 0 \\ k_2 = 0 \end{cases} \tag{23}$$

According to (21), (22) and (23), The reference current value i_{ref} in $\alpha\beta$-axis for flexible power regulation with active power ripple elimination can be obtained by:

$$\begin{cases} i_{\alpha ref} = \dfrac{p_{ref} e_\beta{}'}{e_\alpha e_\beta{}' - e_\alpha{}' e_\beta} + \dfrac{2q_{ref} e_\beta}{e_\alpha{}^2 + e_\beta{}^2 + e_\beta{}'^2 + e_\alpha{}'^2} \\ i_{\beta ref} = \dfrac{-p_{ref} e_\alpha{}'}{e_\alpha e_\beta{}' - e_\alpha{}' e_\beta} - \dfrac{2q_{ref} e_\alpha}{e_\alpha{}^2 + e_\beta{}^2 + e_\beta{}'^2 + e_\alpha{}'^2} \end{cases} \tag{24}$$

B. Current Calculation of Flexible Power Regulation With Reactive Power Ripple Elimination

GC-BVSC can not only generate active power but also has the capability to regulate reactive power. In this part, the control objective of flexible power regulation with eliminating reactive power ripple. The GC-BVSC works as a reactive power generator. In order to eliminate the reactive power ripple, q_{c2} and q_{s2} in the corresponding formula (21) are 0. Thus, the coefficients k_3 and k_4 are 0. It is equivalent to solve the following equation:

$$\begin{cases} p_0 = P_{ref} \\ q_0 = Q_{ref} \\ k_3 = 0 \\ k_4 = 0 \end{cases} \tag{25}$$

According to (21), (22) and (24), the current reference value i_{ref} in $\alpha\beta$-*axis* for power regulation with reactive power ripple elimination can be obtained by:

$$\begin{cases} i_{\alpha ref} = \dfrac{2P_{ref} e_\alpha}{e_\alpha{}^2 + e_\beta{}^2 + e_\alpha{}'^2 + e_\beta{}'^2} - \dfrac{e'_\alpha}{e_\alpha e'_\beta - e'_\alpha e_\beta} Q_{ref} \\ i_{\beta ref} = \dfrac{2P_{ref} e_\beta}{e_\alpha{}^2 + e_\beta{}^2 + e_\alpha{}'^2 + e_\beta{}'^2} - \dfrac{e'_\beta}{e_\alpha e'_\beta - e'_\alpha e_\beta} Q_{ref} \end{cases} \tag{26}$$

Equations (24) and (26) are current reference values for different control objectives. Only one of them is needed in the implementation with the digital signal processor. Without PLL and sequence extraction, the calculation amount in this method is highly reduced under unbalanced grid voltages.

C. IMPCC Cost Function With Delay Compensation

It can be seen from (24) and (26) that the reference current values are expressed by grid voltage with their quadrature signals in the $\alpha\beta$ stationary coordinates system.

In order to select the optimal switching vector and realize IMPCC, the cost function g is established as follow:

$$\begin{aligned} g = &|i_{\alpha ref} - i_\alpha(k+1)| + |i_{\beta ref} - i_\beta(k+1)| \\ &+ \lambda \left[|P_{ref} - P(k+1)| + |Q_{ref} - Q(k+1)|\right] \end{aligned} \tag{27}$$

Where λ is a weighting coefficient, the first and second terms in the cost function penalize the grid-connected current distortion. The third and fourth terms are used to minimize the power ripple.

In the digital implementation, there is usually one step delay between the selected voltage vector and the applied voltage vector, which has a significant influence on the dynamic and static performance of the system [25]. To compensate the one step delay in the digital control, the cost function considering the tracking error at (k + 2)th instant should be evaluated and minimized to select the best voltage vector, which is:

$$\begin{aligned} g = &|i_{\alpha ref} - i_\alpha(k+2)| + |i_{\beta ref} - i_\beta(k+2)| \\ &+ \lambda \left[|P_{ref} - P(k+2)| + |Q_{ref} - Q(k+2)|\right] \end{aligned} \tag{28}$$

The predictive power and current at (k + 2)th sampling period can be calculated from (k + 1)th sampling instant as:

$$\begin{aligned} \begin{bmatrix} P(k+2) \\ Q(k+2) \end{bmatrix} = &\frac{T_s}{L} \begin{bmatrix} e_\alpha & e_\beta \\ e_\beta & -e_\alpha \end{bmatrix} \\ &\times \begin{bmatrix} u_\alpha(k+1) - e_\alpha - Ri_\alpha(k+1) \\ u_\beta(k+1) - e_\beta - Ri_\beta(k+1) \end{bmatrix} \\ &+ \begin{bmatrix} P(k+1) \\ Q(k+1) \end{bmatrix} \end{aligned} \tag{29}$$

$$\begin{aligned} \begin{bmatrix} i_\alpha(k+2) \\ i_\beta(k+2) \end{bmatrix} = &\frac{T_s}{L} \begin{bmatrix} u_\alpha(k+1) - e_\alpha \\ u_\beta(k+1) - e_\beta \end{bmatrix} \\ &+ \left(1 - \frac{RT_s}{L}\right) \begin{bmatrix} i_\alpha(k+1) \\ i_\beta(k+1) \end{bmatrix} \end{aligned} \tag{30}$$

The block diagram of the proposed IMPCC is shown in Fig. 4. The grid voltage and current e_α, e_β, i_α, i_β in the $\alpha\beta$ stationary coordinates are obtained by Clark transformation on e_a, e_b, e_c, i_a, i_b, and i_c. Then, $e_\alpha{}'$ and $e_\beta{}'$ are obtained by lagging 90° of e_α and e_β. The reference current values $i_{\alpha ref}$, $i_{\beta ref}$ are calculated by (24) or (26). The converter output voltage u_α and u_β are obtained by (5). Predictive functions (7), (10) output predictive values of $i_\alpha(k+1)$, $i_\beta(k+1)$, $P(k+1)$, $Q(k+1)$. Delay compensation functions (29), (30) calculate $(k+2)$th predictive values $i_\alpha(k+2)$, $i_\beta(k+2)$, $P(k+2)$, $Q(k+2)$.

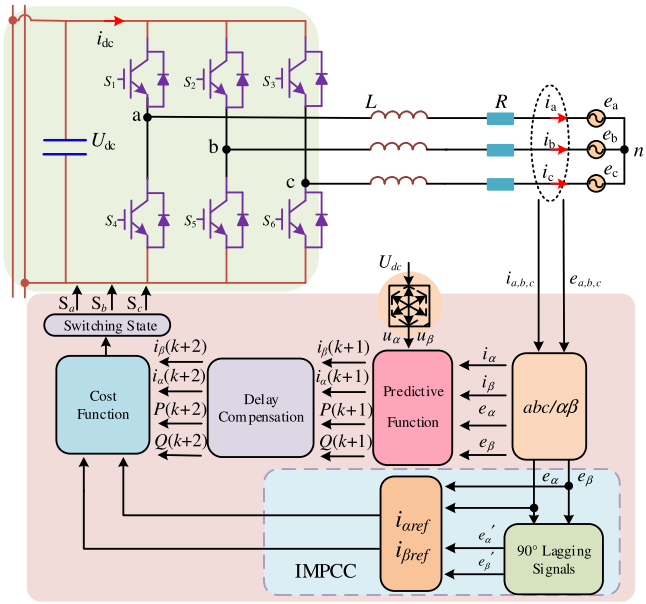

Fig. 4. Block diagram of the proposed IMPCC.

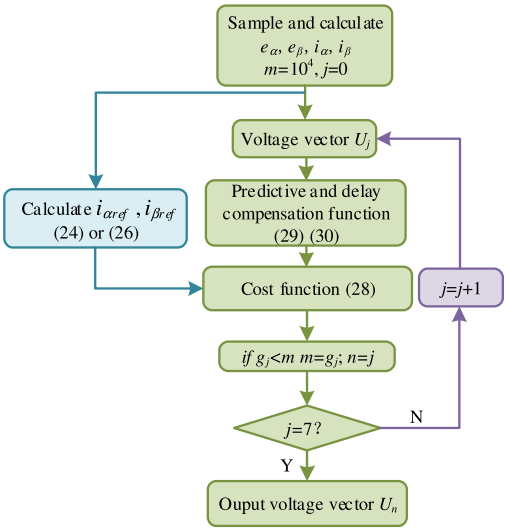

Fig. 5. Flow chart of the proposed IMPCC scheme.

TABLE I
SYSTEM PARAMETERS OF GC-BVSC

Symbol	System Parameters	Value
R	line resistance	0.2 Ω
U_{dc}	DC-side voltage	350 V
C	DC-side capacitance	3000 μF
L	filter inductance	10 mH
e	grid line-line voltage(RMS)	150 V
λ	weighing factor	0.004
f	Line frequency	50 Hz
f_{samp}	sampling frequency	20 kHz

The cost function (28) is used to evaluate the voltage vectors and select the switching state S_a, S_b, S_c, which minimizes the cost function. The flow chart of the IMPCC algorithm is shown in Fig. 5.

V. SIMULATION RESULTS

The simulation in Matlab/Simulink environment is set up to verify the proposed IMPCC method under unbalanced grid voltage conditions. The system parameters are listed in Table I. In this paper, the simulation results obtained from conventional MPCC and the proposed IMPCC are presented for comparison under unbalanced grid voltage conditions.

Figs. 6 and 7 show the simulation results of the transition process from the balanced grid to unbalanced grid voltages, when GC-BVSC works in inverter mode and generates inductive reactive power, using MPCC and IMPCC, respectively. Before 0.05 s, the reference power P_{ref} is 1000 W, and Q_{ref} is −1000 Var. At 0.05 s, the amplitude of phase A dips 20%. In Fig. 6(a), the total harmonic distortion (THD) of grid currents is 1.43% in the balanced grid and 4.26% in the single-phase unbalanced grid voltages. After voltage dips, there are also twice line-frequency power ripple both in active power and reactive power. However, in Fig. 6(b), with IMPCC, the current THD is only 1.46%, which are not deteriorated under the unbalanced

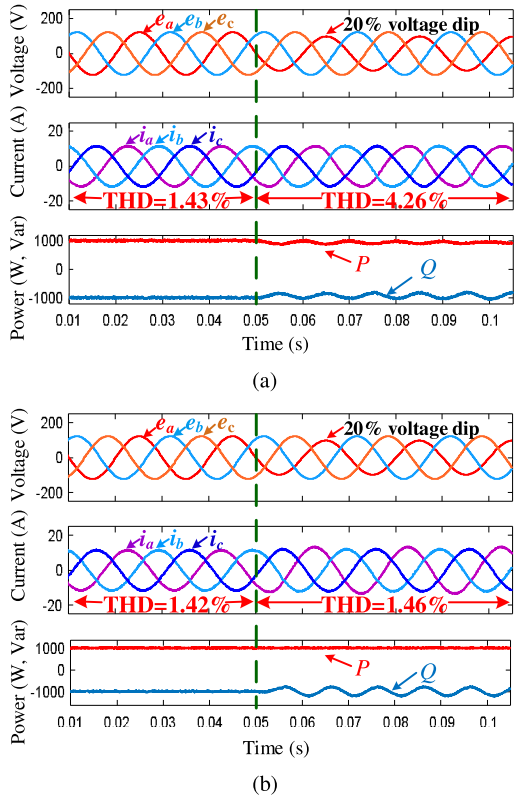

Fig. 6. Simulation results from balanced grid to one-phase unbalanced grid in inverter mode with active power ripple elimination, (a) MPCC, (b) IMPCC.

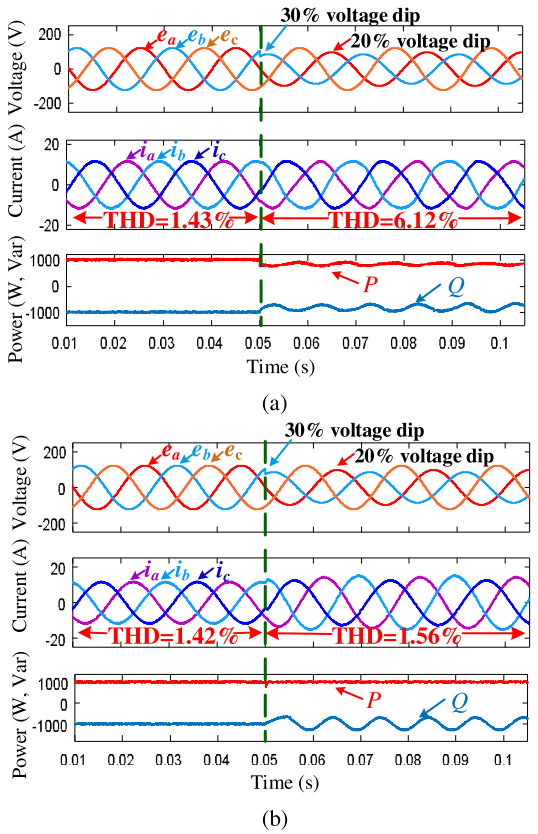

Fig. 7. Simulation results from balanced grid to three-phase unbalanced grid in inverter mode with active power ripple elimination, (a) MPCC, (b) IMPCC.

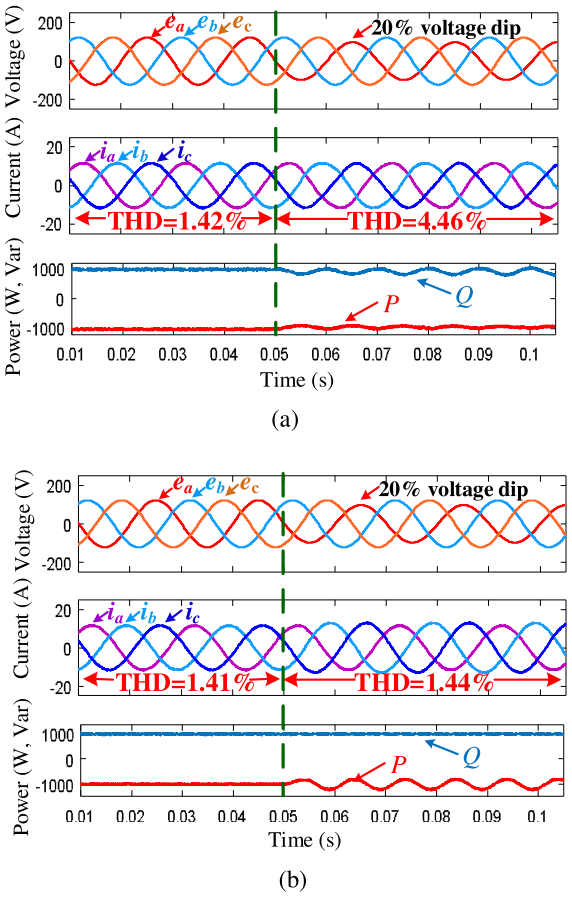

Fig. 8. Simulation results from balanced grid to one-phase unbalanced grid in rectifier mode with reactive power ripple elimination, (a) MPCC, (b) IMPCC.

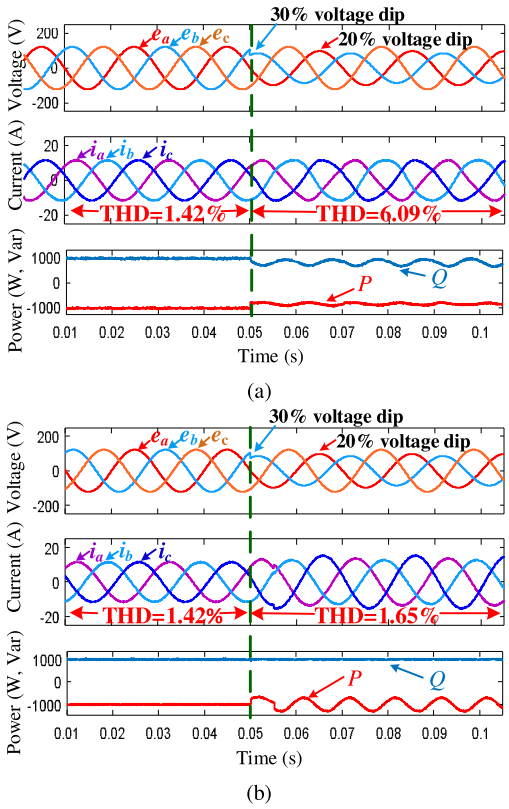

Fig. 9. Simulation results from balanced grid to three-phase unbalanced grid in rectifier mode with reactive power ripple elimination, (a) MPCC, (b) IMPCC.

grid voltage conditions. There is also no twice line-frequency power ripple in active power with IMPCC.

In Fig. 7, at 0.05 s, the voltage amplitude of phase A and phase B dips 20% and dips 30%, respectively. The grid voltages are three-phase unbalanced. In Fig. 7(a), the grid currents THD is 1.43% in the balanced grid and 6.12% in the unbalanced grid. After voltage sags, there are also twice line-frequency power ripple both in active power and reactive power. In Fig. 7(b), with IMPCC, when unbalanced voltages occur, the current THD is only 1.56% and twice line-frequency power ripple in active power are eliminated with IMPCC.

Figs. 8 and 9 show the simulation results of the transition process from the balanced grid to unbalanced grid, when the GC-BVSC works in rectifier mode and generates capacitive reactive power. Before 0.05 s, the reference power P_{ref} is -1000 W, and Q_{ref} is 1000 Var. In Fig. 8, at 0.05 s, the voltage amplitude of phase A dips 20%. Current THD with MPCC are 1.42% in the balanced grid and 4.46% in one-phase unbalanced grid voltages, as shown in Fig. 8(a). However, current THD with IMPCC are reduced to 1.41% under balanced grid voltages and 1.44% after voltage drops, as shown in Fig. 8(b). The current THD is lower with IMPCC than with MPCC. Furthermore, after 0.05 s, there is twice line-frequency power ripple in both active power and reactive, as shown in Fig. 8(a). But the reactive power ripple can be eliminated with IMPCC, as shown in Fig. 8(b).

In Fig. 9, the reference power values are P_{ref} is -1000 W, and Q_{ref} is 1000 Var. At 0.05 s, the voltage amplitude of phase A and B dips 20% and 30%, respectively. Current THD with MPCC is 1.42% in the balanced grid and 6.09% in three-phase unbalanced grid voltages, as shown in Fig. 9(a). Current THD with IMPCC is still 1.42% under balanced grid. However, under three-phase unbalanced grid, current THD with IMPCC is reduced to 1.65%, as shown in Fig. 9(b).

Compared to conventional MPCC, the current waveforms with IMPCC are sinusoidal with less current harmonics components. The current THD are significantly reduced with IMPCC, which has lower harmonic interference to the grid. In addition, in the steady-state simulation, there is twice line-frequency power ripple under unbalanced grid voltages with conventional MPCC. The ripple in active power or reactive power can be eliminated with different control objective using IMPCC. The power quality is improved and simulation results indicate that IMPCC has better performance in steady states. More comparison with VOC and DPC will be discussed in experimental verification.

VI. Experimental Verification

In order to further verify the proposed control strategy performance, a GC-BVSC experimental setup based on power electronics-professional (PE-PRO) is built up and the photograph of the experimental setup is shown in Fig. 10. Control system is implemented by TI TMS320F28335 and IGBT 7MBP50RJ120. The test instrument is composed of YOKO-

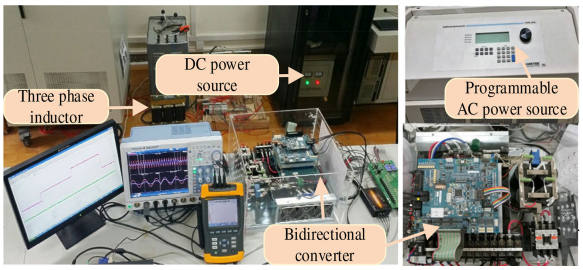

Fig. 10. Experimental setup of GC-BVSC under unbalanced grid voltage.

TABLE II
GRID-CONNECTED CURRENTS THD WITH ACTIVE POWER REGULATION

Condition		VOC	MPCC	DPC	Proposed IMPCC
One-phase voltage sag	Inverter mode	4.2%	4.2%	2.7%	2.3%
	Rectifier mode	3.6%	4.0%	2.9%	2.4%
Two-phase voltage sag	Inverter mode	5.9%	5.9%	2.7%	2.4%
	Rectifier mode	5.6%	5.4%	3.0%	2.6%

GAWA DLM4000 series mixed signal oscilloscope, FLUKE 435B power quality analyzer, and APL-II DC power supply. The Amteke MX30 programmable AC power source is used to emulate unbalanced grid voltages. The experimental parameters are shown in Table II.

A. Dynamic Response of Transition From Inverter Mode to Rectifier Mode Under Unbalanced Grid Voltages

Fig. 11 shows the experimental results of bidirectional active power conversion between inverter mode and rectifier mode under one-phase unbalanced grid voltages. The voltage amplitude of phase A dips 20%. Before 0.05 s, the reference power p_{ref} is 1000 W and q_{ref} is −1000 Var. The GC-BVSC works in inverter mode and generates inductive reactive power. At 0.05 s, p_{ref} steps from 1000 to −1000 W and the GC-BVSC works in rectifier mode. Fig. 11(a) and (b) show the results with VOC and MPCC, respectively. The grid current THD are both 4.2% in the inverter mode and 3.6%, 4.0% in the rectifier mode, respectively. There are twice line-frequency power ripples in both active power and reactive power with the VOC and MPCC. The results of the model predictive DPC method [21] and the proposed IMPCC with eliminating active power ripple are shown in Fig. 11(c) and (d). The grid current THD drops to 2.7%, 2.3% in the inverter mode and 2.9%, 2.4% in the rectifier mode, respectively. With these two schemes, the converter can track active power with reference power and the active power ripple is eliminated.

Fig. 12 shows the experimental results of transition between inverter mode and rectifier mode under three-phase balanced grid voltages. The voltages of phase A and phase B drop 20% and 30% of the normal voltage, respectively. The current distortion

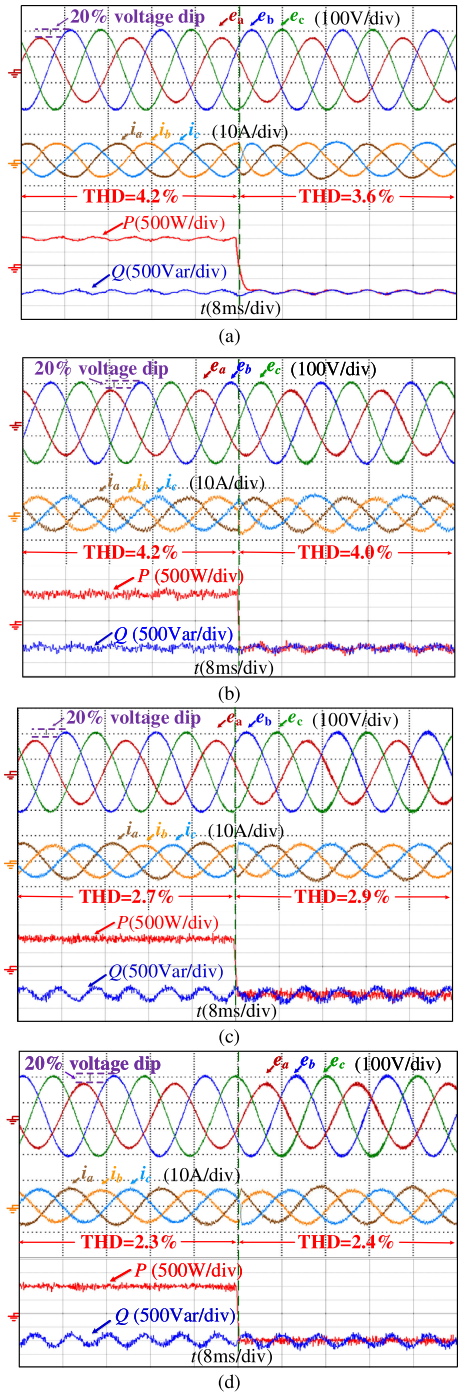

Fig. 11. Under one-phase unbalanced grid voltages, experimental results of the transition between inverter mode and rectifier mode (eliminating active power ripple), using (a) VOC (b) MPCC (c) DPC (d) IMPCC.

and power ripple become larger for the VOC and MPCC, which are both 5.9% in inverter mode and 5.6%, 5.4% in the rectifier mode. The current THD is reduced to 2.7%, 2.4% in inverter mode and 3.0%, 2.6% in rectifier mode with model predictive DPC and IMPCC, respectively. At the same time, the twice line-frequency ripple of the active power is eliminated. The experimental results of current THD in these two unbalanced conditions are shown in Table II.

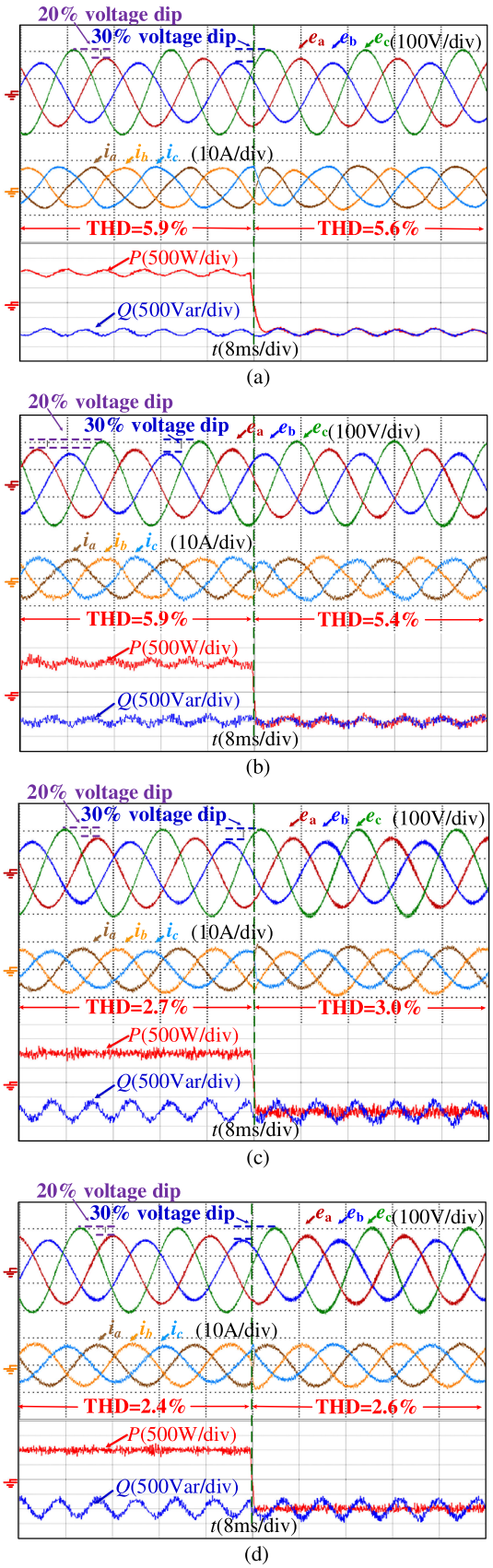

Fig. 12. Under three-phase unbalanced grid voltages, experimental results of the transition between inverter mode and rectifier mode (eliminating active power ripple), using (a) VOC (b) MPCC (c) DPC (d) IMPCC.

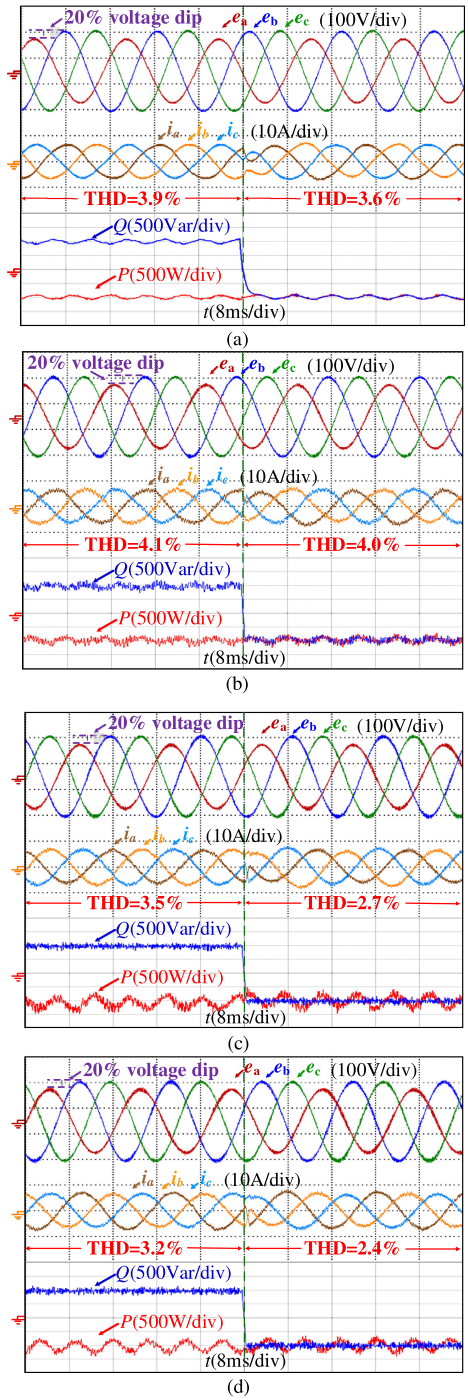

Fig. 13. Under one-phase unbalanced grid voltages, experimental results of the transition of reactive power regulation in rectifier mode with eliminating reactive power ripple, using (a) VOC (b) MPCC (c) DPC (d) IMPCC.

B. Dynamic Responses of Reactive Power Regulation Under Unbalance Grid Voltage Conditions

In the condition of unbalanced grid voltages, the dynamic responses of reactive power regulation in rectifier mode are investigated. Fig. 13 shows the experimental results under 20% voltage dip in one-phase. Before 0.05 s, the reference power p_{ref} is -1000 W, and q_{ref} is 1000 Var. The GC-BVSC works in rectifier mode and generates capacitive reactive power. At

0.05 s, Q_{ref} steps from 1000 to −1000 Var, and the GC-BVSC begins to generate inductive reactive power.

As shown in Fig. 13(a) and (b), the grid currents with conventional VOC and MPCC have serious distortion of 3.9%, 4.1% harmonics before reactive power changing and 3.6%, 4.0% harmonics after that. There are twice line-frequency power ripples in both active and reactive power. In the same condition, the converter has better performance with model predictive DPC and IMPCC, and reactive power ripple elimination is achieved which is shown in Fig. 13(c) and (d). The grid currents are sinusoidal and THD drops to 3.5%, 3.2% before reactive power changes and 2.7, 2.4% after that. The power converter can regulate the reactive power to the reference value and keep steady.

Fig. 14 shows the experimental results when the three-phase voltages are all different. At 0.05 s, the voltages of phase A and phase B drop 20% and 30% of the normal voltage, respectively. With the VOC and MPCC, the grid current THD are 5.5%, 5.8% before reactive power changes and from 5.6% to 5.4% after that.

However, by using the model predictive DPC and proposed IMPCC, the output reactive power of the GC-BVSC tracks the reference power value well and the ripple is eliminated. The current THD is 3.6%, 3.3% harmonics with capacitive reactive power generation and 3.2%, 2.7% with inductive power generation. The experimental results for current THD in these two unbalanced conditions are shown in Table III.

C. Fault Voltage Ride-Through (FVRT) Control Strategy

The GC-BVSC is the connection between the DC side and AC grid. When there is voltage sag in AC grid, the GC-BVSC should have the FVRT capability with high power quality. The proposed control scheme can provide the low current THD in unbalanced grid conditions and eliminate the twice line-frequency power ripples. However, when there is a voltage sag fault, the phase current will increase to track the reference power. Therefore, the current limitation technique should be considered to guarantee the safety operation under unbalanced grid conditions.

The peak values of the three-phase current are analyzed and a novel current limitation control method is proposed to achieve flexible power regulation in a safe current operation area under grid faults [30]. A simplified current limitation technique is designed for the current-limited control of grid-connected inverter under unbalanced grid voltage faults. Under unbalanced grid conditions, the GC-BVSC can work with lower THD and power ripples elimination. However, if the GC-BVSC works in the constant power mode, due to the grid voltage drop, the output current will increase. For the safe operation of the GC-BVSC, the current limitation need to be investigated. Based on this conclusion in [30], a simplified current limitation technique for the BVSC application is designed. According to the different depth of the voltage drop, the maximum magnitude of phase current $I_{\max}$ is calculated by (24). Considering the current limitation, when the currents exceed the rated value, the limited reference currents are expressed as:

$$\begin{cases} i_{\alpha ref-limt} = i_{\alpha ref} \cdot \frac{I_{rated}}{I_{\max}} \\ i_{\beta ref-limt} = i_{\beta ref} \cdot \frac{I_{rated}}{I_{\max}} \end{cases} \tag{31}$$

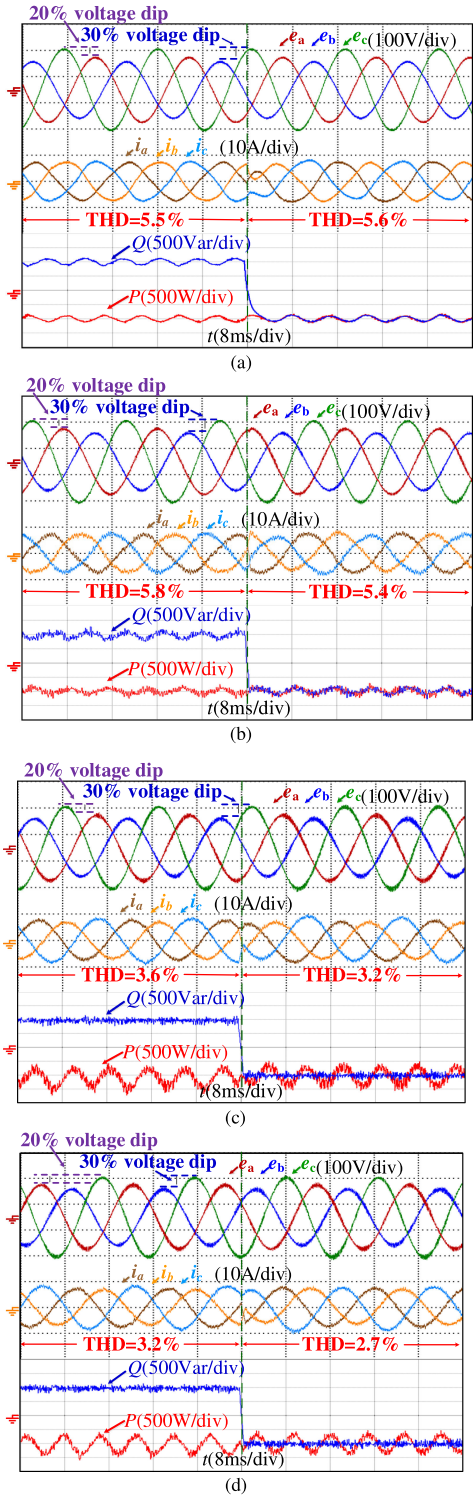

Fig. 14. Under three-phase unbalanced grid voltages, experimental results of the transition between reactive power compensation modes with eliminating reactive power ripple, using (a) VOC (b) MPCC (c) DPC (d) IMPCC.

where I_{rated} is the magnitude of the rated phase current, $I_{\max}$ represents the maximum phase current value in three phase grid-connected current. $I_{\max} = \max(i_a, i_b, i_c)$. According to (31), the magnitude of the phase current will not be larger than I_{rated} under unbalanced grid voltage conditions.

TABLE III
GRID-CONNECTED CURRENTS THD WITH REACTIVE POWER REGULATION

Condition		VOC	MPCC	DPC	Proposed IMPCC
One-phase voltage sag	Capacitive reactive power generation	3.9%	4.1%	3.5%	3.2%
	Inductive reactive power generation	3.6%	4.0%	2.7%	2.4%
Two-phase voltage sag	Capacitive reactive power generation	5.5%	5.8%	3.6%	3.2%
	Inductive reactive power generation	5.6%	5.4%	3.2%	2.7%

TABLE IV
MAXIMUM MAGNITUDE OF PHASE CURRENT

Voltage dip	0–10%	10–20%	20–30%	30–40%	40–50%
$I_{\max}$(A)	9.6	10.3	10.8	12.0	13.2

To verify the effectiveness of the current limitation control strategy. Experiments are conducted by comparing the results before and after current limitation. When the power converter works with unity power factor, the reference active power P_{ref} is 2 kW. The maximum magnitude of phase current with different voltage dip is listed in Table. IV.

The magnitude of the rated phase current is 10 A. When there is the 50% voltage dip in phase A, the experimental results with the proposed IMPCC are shown in Fig. 15(a). The phase current is larger than the rated current value. Fig. 15(b) shows the experimental result with the current limitation design. The grid current is restricted smaller than the rated current value. In addition, to limit the phase current, the output power is also lower than the reference power. Experimental results show that with the current-limited control, the GC-BVSC can work within the safe current operation range. The active power ripple can also be eliminated. Therefore, with the proposed IMPCC, the GC-BVSC can work with lower current THD and power ripples in safe current-limited mode under unbalanced grid conditions.

In Fig. 15(c), before 0.032 s, the active power is 1 kW with unity power factor. At 0.032 s, there is a single-phase voltage sag of 50%. Then, the GC-BVSC work in FVRT mode. The reference active power is regulated to 0, and the reference reactive power is regulated to 1 kVar gradually with a given slope coefficient. The experimental results show that with the FVRT control, the GC-BVSC generates an increased reactive power to keep voltage level, when the grid has a voltage sag fault. The reactive power can be flexibly regulated with power ripple elimination. In addition, the grid current can be controlled well. The IMPCC can provide the FVRT capability to withstand the voltage sags and remains connection to the AC grid. The voltage collapse can be avoided by flexible reactive power generation to support the grid voltage. As a result, the GC-BVSC is able to be connected to the AC grid during grid voltage faults without disconnection between the DC side and AC grid.

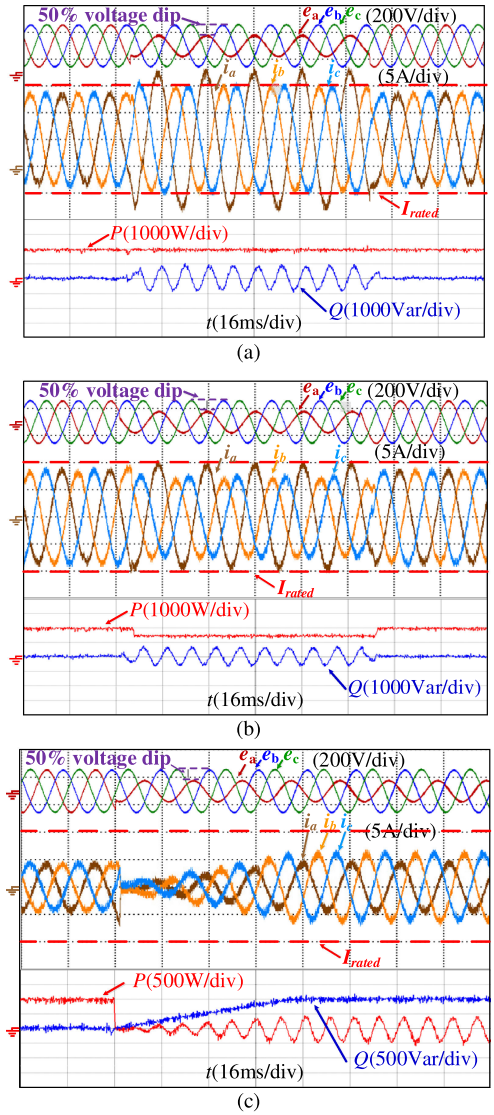

Fig. 15. Under three-phase unbalanced grid voltages, experimental results of the fault ride-though capability (a) without current limitation (b) with current limitation (c) flexible reactive power generation.

D. Comparison Between the Proposed IMPCC and Existing Methods

To show the difference and relationship between the presented IMPCC and existing methods, the comparison has been made in Table V.

A MPC scheme for the dual -mode Z-source inverter and voltage source inverter with seamless transition between grid-connected and islanding mode is proposed in [31], [32]. The proposed direct decoupled active and reactive power control can provide the reactive power function. However, it only considers the balanced grid voltage conditions. Under unbalanced grid voltage conditions, twice line frequency power ripples exist and the current THD is also highly increased. As a result, the control scheme should be modified in these conditions.

The decoupled active and reactive power MPC control technique for single-phase grid-tied inverter is presented in [33], [34]. It minimizes the number of the switching state transitions

TABLE V
COMPARISON BETWEEN THE PROPOSED AND EXISTING CONTROL SCHEMES

	VOC [12], [13]	MPDPC [22]	MPC [31], [32]	DPC [19], [20]	Proposed IMPCC
Three-phase unbalance	Yes	Yes	No	Yes	Yes
d-q transformation	Required	Not Required	Not required	Required	Not Required
Current THD	Low	High	Low	Medium	Low
Phase lock loop	Required	Required	Required	Required	Not Required
Power Ripple	High	Low	Medium	Low	Low
Sequence extraction	Required	Required	Not Required	Required	Not Required
Fault current limitation	No	No	No	No	Yes

and reduces the switching frequency and power losses. An adaptive weight factor is designed which minimizes the tracking error and switching frequency. However, if it is applied in the three-phase grid network, the control scheme need to be modified.

A combined wind farm controller based on the MPC is proposed to improve the voltage control [35]. The proposed method is applied to the normal and emergency conditions of the wind farm. It provides the reference power to the grid-connected converters. However, it is a system-level control for the wind farm and cannot be used in the converter-level control directly.

Under unbalanced grid voltage conditions, DPC control schemes which can regulate both the positive- and negative-sequence currents have been introduced to deal with these problems [19], [20]. An improved MPDPC for PWM rectifiers is proposed in [21]. The power converter can work with unity power factor, and the reactive power regulation is not investigated in detail. The low-complexity model predictive direct power control in [22] achieves flexible power control under unbalanced grid conditions. However, the phase locked loop and sequence extraction are still necessary to implement the control scheme, which can be further improved.

The IMPCC is similar to the MPDPC, and they both select one voltage vector for the next control period, but their vector selection principles are entirely different. According to the control objectives of eliminating the ripples in active power or reactive power, the compensation current can be calculated by the IMPCC. A cost function reducing both the power ripple and current THD is designed to evaluate the effects of different voltage vectors. Then, the vector which minimizes the cost function will be adopted. Compared to the MPDPC and DPC, the vector selected from the IMPCC is more accurate and efficient in the conditions of unbalanced grid voltages.

According to the experimental results, under unbalanced grid voltage conditions, there are twice line-frequency power ripples with VOC and MPCC schemes, which can also be analyzed by (14) and (15). p_{c2}, p_{s2}, q_{c2} and q_{s2} will exist in the output power in the unbalanced grid. With the model predictive DPC and the proposed IMPCC, the twice line-frequency power ripples which exist in active power or reactive power can be eliminated. Therefore, the output power can be controlled stable. In addition, compared to the model predictive DPC [21], the cost function with the proposed IMPCC considers both the reduction of the current THD and power ripple. As a result, the current THD of the IMPCC is lower, which has been verified by the experimental results.

Due to the calculation of both the current and power, the calculation burden is larger than the model predictive DPC, which only evaluates the power error in the cost function. In the experiments, the IMPCC algorithm execution time is 0.018 ms, which costs 2698 computing cycles of TMS320 F28335. Fortunately, similar to the model predictive DPC, without coordinate transformation from $\alpha\beta$ to dq rotating frame, the PLL, positive- and negative- sequence separation, and PWM module are not needed. In IMPCC, the current limitation is considered for the safe operation of GC-BVSC, and flexible reactive power generation can also be achieved.

VII. CONCLUSION

In the condition of unbalanced grid voltages, this paper proposes an IMPCC scheme with delay compensation for GC-BVSC with high power quality. The reference currents of IMPCC are expressed by grid voltages and their quadrature signals in the $\alpha\beta$ stationary coordinates system without Park transformation. Moreover, the cost function is a measurement of both power ripple and current distortion. Under both single phase and three phase unbalanced grid voltages, based on a PE-PRO platform, it has been shown with experiments that IMPCC keeps the grid-connected current sinusoidal. It also has been demonstrated with experimental results the ripple of active power or reactive power can be eliminated with different control objectives.

The proposed method does not need positive and negative sequence separation, and PLL and PWM modulation. As a result, the computation complexity is greatly reduced. Compared to the traditional MPCC and VOC scheme, IMPCC improves the power quality with reduced current distortion and power ripple under the unbalanced grid, which has less harmonic currents interference to other equipments and customers with flexible power regulation. With the current limited control design, the power converter works in the safe area without over-current operation under unbalanced voltage conditions. In addition, experimental results also show that the IMPCC achieves a good dynamic performance of bidirectional power conversion with flexible reactive power compensation capability. The proposed method provides a simple and effective method to improve the power quality and guarantee the safe operation for the GC-BVSC under unbalanced grid voltage conditions.

REFERENCES

[1] P. Wang, C. Jin, D. Zhu, Y. Tang, P. C. Loh, and F. H. Choo, "Distributed control for autonomous operation of a three-port AC/DC/DS hybrid microgrid," *IEEE Trans. Ind. Electron*, vol. 62, no. 2, pp. 1279–1290, Feb. 2015.

[2] T. Ma, M. H. Cingle, and O. A. Mohammed, "Control of a hybrid AC/DC microgrid involving energy storage and pulsed loads," *IEEE Trans. Ind. Appl.*, vol. 53, no. 1, pp. 567–575, Jan./Feb. 2017.

[3] K. Sun, X. Wang, Y. W. Li, F. Nejabatkhah, Y. Mei, and X. Lu, "Parallel operation of bidirectional interfacing converters in a hybrid AC/DC microgrid under unbalanced grid voltage conditions," *IEEE Trans. Power Electron.*, vol. 32, no. 3, pp. 1872–1884, Mar. 2017.

[4] Y. Gu, X. Xiang, W. Li, and X. He, "Mode-adaptive decentralized control for renewable DC microgrid with enhanced reliability and flexibility," *IEEE Trans. Power Electron.*, vol. 29, no. 9, pp. 5072–5080, Sep. 2014.

[5] Z. Wang, W. Wu, and B. Zhang, "A distributed control method with minimum generation cost for DC microgrids," *IEEE Trans. Energy Convers.*, vol. 31, no. 4, pp. 1462–1470, Dec. 2016.

[6] X. Chang, Y. Li, X. Li, and X. Chen, "An active damping method based on a supercapacitor energy storage system to overcome the destabilizing effect of instantaneous constant power loads in DC microgrids," *IEEE Trans. Energy Convers.*, vol. 32, no. 1, pp. 36–47, Mar. 2017.

[7] F. Nejabatkhah and Y. W. Li, "Overview of power management strategies of hybrid AC/DC microgrid," *IEEE Trans. Power Electron.*, vol. 30, no. 12, pp. 7072–7089, Dec. 2015.

[8] Y. H. Liao and H. C. Chen, "Simplified PWM with switching constraint method to prevent circulating currents for paralleled bidirectional AC/DC converters in grid-tied system using graphic analysis," *IEEE Trans. Ind. Electron.*, vol. 62, no. 7, pp. 4573–4586, Jul. 2015.

[9] Y. Zhang and C. Qu, "Direct power control of a pulse width modulation rectifier using space vector modulation under unbalanced grid voltages," *IEEE Trans. Power Electron.*, vol. 30, no. 10, pp. 5892–5901, Oct. 2015.

[10] Y. Zhang and C. Qu, "Table-based direct power control for three-phase AC/DC converters under unbalanced grid voltages," *IEEE Trans. Power Electron.*, vol. 30, no. 12, pp. 7090–7099, Dec. 2015.

[11] H. C. Chen and J. Y. Liao, "Bidirectional current sensorless control for the full-bridge AC/DC converter with considering both inductor resistance and conduction voltages," *IEEE Trans. Power Electron.*, vol. 29, no. 4, pp. 2071–2082, Nov. 2014.

[12] R. Teodorescu, M. Liserre, and P. Rodriguez, *Grid Converters for Photovoltaic and Wind Power Systems*. New York, NY, USA: Wiley-IEEE, 2011.

[13] P. Rodriguez, A. Luna, R. Munoz-Aguilar, I. Etxeberria-Otadui, R. Teodorescu, and F. Blaabjerg, "A stationary reference frame grid synchronization system for three-phase grid-connected power converters under adverse grid conditions," *IEEE Trans. Power Electron.*, vol. 27, no. 1, pp. 99–112, Jan. 2012.

[14] C. H. Ng, L. Ran, and J. Bumby, "Unbalanced-grid-fault ride-through control for a wind turbine inverter," *IEEE Trans. Ind. Appl.*, vol. 44, no. 3, pp. 845–856, May/Jun. 2008.

[15] P. Rodriguez, A. V. Timbus, R. Teodorescu, M. Liserre, and F. Blaabjerg, "Flexible active power control of distributed power generation systems during grid faults," *IEEE Trans. Ind. Electron.*, vol. 54, no. 5, pp. 2583–2592, Oct. 2007.

[16] J. Alonso-Martínez, J. E. G. Carrasco, and S. Arnaltes, "Table-based direct power control: A critical review for microgrid applications," *IEEE Trans. Power Electron.*, vol. 25, no. 12, pp. 2949–2961, Dec. 2010.

[17] Y. Zhang and J. Zhu, "Direct torque control of permanent magnet synchronous motor with reduced torque ripple and commutation frequency," *IEEE Trans. Power Electron.*, vol. 26, no. 1, pp. 235–248, Jan. 2011.

[18] H. Nian, Y. Shen, H. Yang, and Y. Quan, "Flexible grid connection technique of voltage-source inverter under unbalanced grid conditions based on direct power control," *IEEE Trans. Ind. Appl.*, vol. 51, no. 5, pp. 4041–4050, Sep. 2015.

[19] J. Eloy-Garcia, S. Arnaltes, and J. L. Rodriguez-Amenedo, "Direct power control of voltage source inverters with unbalanced grid voltages," *IET Power Electron*., vol. 1, no. 3, pp. 395–407, Sep. 2008.

[20] L. Shang, D. Sun, and J. Hu, "Sliding-mode-based direct power control of grid-connected voltage-sourced inverters under unbalanced network conditions," *IET Power Electron*., vol. 4, no. 5, pp. 570–579, May 2011.

[21] Y. Zhang and C. Qu, "Model predictive direct power control of PWM rectifiers under unbalanced network conditions," *IEEE Trans. Ind. Electron.*, vol. 62, no. 7, pp. 4011–4022, Jul. 2015.

[22] D. Sun and X. Wang, "Low-complexity model predictive direct power control for DFIG under both balanced and unbalanced grid conditions," *IEEE Trans. Ind. Electron.*, vol. 63, no. 8, pp. 5186–5196, Aug. 2016.

[23] K. Ma, W. Chen, M. Liserre, and F. Blaabjerg, "Power controllability of a three-phase converter with an unbalanced AC source," *IEEE Trans. Power Electron.*, vol. 30, no. 3, pp. 1591–1604, Mar. 2015.

[24] J. Nan, H. Shiyang, C. Guangzhao, J. Suxia, and K. Dongyi, "Model-predictive current control of grid-connected inverters for PV systems," in *Proc. Int. Conf. Renewable Power Gener.*, Oct. 2015, pp. 1–5.

[25] P. Cortes, J. Rodriguez, C. Silva, and A. Flores, "Delay compensation in model predictive current control of a three-phase inverter," *IEEE Trans. Ind. Electron.*, vol. 59, no. 2, pp. 1323–1325, Feb. 2012.

[26] J. Hu, J. Zhu, G. Lei, G. Platt, and D. G. Dorrell, "Multi-objective model-predictive control for high-power converters," *IEEE Trans. Energy Convers.*, vol. 28, no. 3, pp. 652–663, Sep. 2013.

[27] S. Kwak and J. C. Park, "Model-predictive direct power control with vector preselection technique for highly efficient active rectifiers," *IEEE Trans. Ind. Informat.*, vol. 11, no. 1, pp. 44–52, Feb. 2015.

[28] M. Narimani, B. Wu, V. Yaramasu, and N. R. Zargari, "Finite control-set model predictive control (FCS-MPC) of nested neutral point-clamped (NNPC) converter," *IEEE Trans. Power Electron.*, vol. 30, no. 12, pp. 7262–7269, Dec. 2015.

[29] J. Rodriguez, M. P. Kazmierkowski, J. R. Espinoza, P. Zanchetta, H. Abu-Rub, and H. A. Young, "State of the art of finite control set model predictive control in power electronics," *IEEE Trans. Ind. Informat.*, vol. 9, no. 2, pp. 1003–1016, May 2013.

[30] X. Guo, W. Liu, and Z. Lu, "Flexible power regulation and current-limited control of grid-connected inverter under unbalanced grid voltage faults," *IEEE Trans. Ind. Electron.*, vol. 64, no. 9, pp. 7425–7432, Sep. 2017.

[31] R. Ahmadi and S. Sajadian, "Model predictive control of dual-mode operations Z-source inverter: Islanded and grid-connected," *IEEE Trans. Power Electron.*, to be published, doi: 10.1109/TPEL.2017.2723358.

[32] X. Li, H. Zhang, M. B. Shadmand, and R. S. Balog, "Model predictive control of a voltage-source inverter with seamless transition between islanded and grid-connected operations," *IEEE Trans. Ind. Electron.*, vol. 64, no. 10, pp. 7906–7918, Oct. 2017.

[33] M. B. Shadmand, X. Li, R. S. Balog, and H. Abu Rub, "Constrained decoupled power predictive controller for a single-phase grid-tied inverter," *IET Renewable Power Gener.*, vol. 11, no. 5, pp. 659–668, 2017.

[34] B. Ge, X. Li, H. Zhang, Y. Liu, R. S. Balog, and H. Abu Rub, "Direct instantaneous ripple power predictive control for active ripple decoupling of single-phase inverter," *IEEE Trans. Ind. Electron.*, to be published, doi: 10.1109/TIE.2017.2750612.

[35] H. Zhao, Q. Wu, J. Wang, Z. Liu, M. Shahidehpour, and Y. Xue, "Combined active and reactive power control of wind farms based on model predictive control," *IEEE Trans. Energy Convers.*, vol. 32, no. 3, pp. 1177–1187, Sep. 2017.

Nan Jin (M'16) received B.S. and M.S. degrees in electrical engineering from the Zhengzhou University of Light Industry, Zhengzhou, China, in 2003 and 2007, respectively, and the Ph.D. degree in power electronics and electrical drives from Shanghai Jiao Tong University, Shanghai, China, in 2012.

He is currently an Associate Professor with the Zhengzhou University of Light Industry. He is also a Visiting Professor with the Department of Electrical Engineering and Computer Science, The University of Tennessee, Knoxville, TN, USA. He has authored or coauthored more than 30 technical papers in journals and conference proceedings, two books, and holds eight Chinese patents. His research interests include model predictive control method for power converter, microgrids, clean energy power conversion, and fault diagnosis and tolerant control of power electronics system.

Chun Gan (S'14–M'16) received the B.S. and M.S. degrees in power electronics and motor drives from the China University of Mining and Technology, Jiangsu, China, in 2009 and 2012, respectively, and the Ph.D. degree in power electronics and motor drives from Zhejiang University, Hangzhou, China, in 2016.

He is currently a Research Associate with the Department of Electrical Engineering and Computer Science, University of Tennessee, Knoxville, TN, USA. He is also a Research Staff with the U.S. Energy/National Science Foundation cofunded Engineering Research Center CURENT. He has authored or coauthored more than 50 technical papers in leading journals and conference proceedings, including more than 20 IEEE Transaction papers, and authored one book chapter. He has 12 issued/published invention patents. His research interests include high-efficiency power converters, electric vehicles, electrical motor drives, electrical motor design, continuous variable series reactors, high-voltage direct current transmission, and microgrids.

Dr. Gan was the recipient of the 2015 Top Ten Excellent Scholar Award, the 2016 Excellent Ph.D. Graduate Award, the 2015 Ph.D. National Scholarship, the 2015 Wang Guosong Scholarship, and the 2014 and 2015 Outstanding Ph.D. Candidate Awards at Zhejiang University.

Leilei Guo (S'13) was born in Henan, China, in 1987. He received the B.S. and Ph.D. degrees in electrical engineering from the School of Electrical Engineering and Automation, Hefei University of Technology, Hefei, China, in 2010 and 2016, respectively.

He is currently working as a Lecturer with the Zhengzhou University of Light Industry, Zhengzhou, China. He has authored or coauthored more than 20 technical papers in journals and conference proceedings, and holds six Chinese patents. His current research interests include model predictive control methods for power converters and permanent-magnet synchronous motors.